Bioprinting 44 (2024) e00368

Contents lists available at ScienceDirect

Bioprinting

journal homepage: www.sciencedirect.com/journal/bioprinting

Double-crosslinked dECM bioink to print a self-sustaining 3D multi-layered aortic-like construct

Federica Potere [a], Giovanni Venturelli [a], Beatrice Belgio [a], Giuseppe Guagliano [b], Federica Boschetti [a,*], Sara Mantero [a], Paola Petrini [b]

[a] Laboratory of Biological Structure Mechanics (LaBS), Department of Chemistry, Materials, and Chemical Engineering "Giulio Natta", Politecnico di Milano, Milano, Italy
[b] Department of Chemistry, Materials and Chemical Engineering "Giulio Natta", Politecnico di Milano, Milano, Italy

ARTICLE INFO

Keywords:
Biofabrication
3D bioprinting
Bioink
Decellularization
Extracellular matrix
Blood vessels

ABSTRACT

Cardiovascular disease is the leading cause of death worldwide, with related mortality increasing from 12.1 million to 18.6 million in the past 30 years.

To address the supply limitation of autologous vascular grafts and overcome the limits of current treatment options, 3D bioprinting techniques have been investigated.

This study aimed at introducing a self-supporting and multi-layered 3D bioprinted construct as a promising alternative for large-blood vessel replacement. To this end, we developed an alginate-gelatin bioink enriched with decellularized extracellular matrix (dECM) of porcine aorta combined with a two-step crosslinking process. We investigated the feasibility of achieving structural stability and shape fidelity of the bioprinted construct over time through rheological characterization, printability tests, and degradation tests.

According to the results of rheology and printability tests, dECM-enriched bioink combined with the double-crosslinking process (internal and external crosslink) showed good printability and high shape fidelity, withstanding more than 35 layers without the need for support. Moreover, the bioprinted construct preserved its structural stability over time, retaining a wall thickness comparable to that of the native aorta. Finally, immortalized mouse fibroblasts embedded in the bioink were well adhered to the bioink and alive over time. The double-crosslinked bioink represents an impactful strategy to produce an alternative conduit with the native hierarchical structure of the large blood vessels.

1. Introduction

Cardiovascular diseases represent the leading cause of death worldwide, causing about 18 million deaths every year [1]. Among these, aortic aneurysms and acute aortic syndromes, such as aortic dissection, are the primary conditions affecting major blood vessels [2–4].

Despite extensive research in the cardiovascular field, care options of vascular disease are still limited. These pathologies are treated with synthetic vascular grafts made of polyethylene terephthalate (PET or Dacron®), polytetrafluoroethylene (PTFE) or expanded polytetrafluoroethylene (ePTFE) [5,6]. Although synthetic grafts often remain the sole viable option [7], their hydrophobic nature hinders the recreation of aqueous cellular environment. Moreover, homografts were initially abandoned due to their immunogenicity, preservation difficulties, delayed degradation, and aneurysm formation [8], they have been reintroduced in specific clinical situations, such as aortic graft infections [9].

The pioneering work by Weinberg and Bell in 1986 introduced the first tissue-engineered blood vessel as an alternative to synthetic grafts [10]. Since then, many fabrication techniques such as electrospinning [11,12], cell-sheet engineering [13], tubular mold casting [14], and xenogeneic vessel decellularization [15] have been used to create tissue-engineered vessels. These techniques involve complex, multi-step processes and manual cell seeding, resulting in uneven cell distribution and failing to accurately replicate the multi-layered structure of native blood vessels with significant anatomic dimensions [16].

Bioprinting holds transformative potential for cardiovascular disease treatment by providing tailored solutions for tissue repair and regeneration [17–19]. This technique allows to fabricate a vessel-like structure

* Corresponding author.
E-mail address: federica.boschetti@polimi.it (F. Boschetti).

https://doi.org/10.1016/j.bprint.2024.e00368
Received 12 August 2024; Received in revised form 18 October 2024; Accepted 23 October 2024
Available online 28 October 2024

in a single step by extruding cell-laden hydrogels with a precise layer-by-layer deposition [20–26].

Natural and synthetic bioinks are employed in 3D bioprinting. Synthetic hydrogels such as polyethileneglicole [27], polycaprolactone [28] and polyvinylpyrrolidone [29], present several limitations that delay their translational applications. These challenges include the use of toxic solvents and difficulties in cell encapsulation. Additionally, synthetic materials typically lack cell recognition sites and other biological cues found in the natural extracellular matrix (ECM), which are essential for promoting cell proliferation and differentiation. While functionalizing synthetic materials can improve their biological properties, the presence of adaptable side groups is crucial for accurately tailoring the mechanical and biological properties of a construct.

Natural hydrogels are commonly used as bioink materials in bioprinting due to their numerous advantageous characteristics that enhance the 3D printing process. Natural polymers have taken on a central role as bioinks for 3D bioprinting of tissues and organs because they provide scaffolding systems suitable for the structural and functional organization of cells. These polymers possess unique properties such as non-toxicity, biocompatibility, and biodegradability, making them ideal for tissue regeneration in various tissue engineering applications [30]. To this, many bioinks have been used to print three-dimensional tubular constructs. Bioinks based on natural materials, such as agarose [31], fibrinogen [5], xanthan gum [32,33], alginate, and gelatin [34,35], offer a hydrophilic environment able to support the regenerative approach hindered with the PET or PTFE grafts [36].

However, natural-based bioinks lack the necessary rheological and mechanical properties to produce vascular constructs with dimensions suitable for large vessels, leading to structural collapse during printing. For instance, Tan et al. developed an alginate-xanthan gum bioink and optimized the printing process by crosslinking the bioink with calcium chloride ($CaCl_2$) during the bioprinting step [33]. Despite these efforts, their attempts to print tubular constructs of varying heights did not fully achieve shape fidelity and height stability. To tackle this issue, the use of functionalized hydrogels, such as gelatin-methacryloyl (GelMA), was explored.

Xu et al. successfully bioprinted vascular structures utilizing a bioink made of GelMA, gelatin, and hyaluronic acid. The bioprinting process involved pneumatic extrusion, with a rather high dispensing pressure of about 100 kPa [16]. Another strategy to reach relevant anatomical dimensions involves the employment of supports during printing: some studies have successfully printed multi-layered vascular constructs within a support bath. In 2021, Dikyol et al. bioprinted multi-layered tubular constructs using an alginate-gelatin bioink extruded into a support bath composed of Pluronic F127, Laponite-RDS, and $CaCl_2$ [37]. Similarly, Ding et al. endeavored to bioprint vascular constructs using an alginate-gelatin bioink within a support bath medium containing Laponite nanoclay and $CaCl_2$ [35]. Additionally, several attempts have been made to fabricate tubular constructs using rotating mandrel-aided bioprinting [3,5,38]. However, these strategies often involve complex multi-step processes, including the removal of support materials, which can affect the stability of the printed structure and cell viability. Hence, obtaining a self-standing tubular hierarchical structure with the dimensions of a native large vessel, while maintaining a cell-friendly environment, remains challenging.

This work aims to biofabricate a self-supporting 3D multi-layered construct able to replicate the native hierarchical and chemical structure, and functionality of the native vascular ECM. To this end, we present a novel bioink made of sodium alginate and gelatin, enriched by dECM, to reproduce the extracellular environment. The biochemical signals within the bioink, composed of ECM components, are hypothesized to play a pivotal role in promoting cell proliferation, while mitigating the risk of thrombosis and inflammation [6,36–41]. The formulation of the new dECM-based bioink is optimized to be suitable for the extrusion-based 3D bioprinting process by *a priori* and post-printing assessment. In fact, rheological tests, printability assessments, and shape fidelity evaluations (including swelling and degradation tests) were conducted to determine the optimal composition of the bioink. These tests were crucial to ensure that the hydrogel could be extruded at pressures that maintained cell viability. Moreover, this work addresses the innovative challenge of preserving the desired shape, specifically replicating the geometry and anatomical structure of the aorta, which is characterized by its three distinct, non-overlapping tunics. Once the optimal bioink formulation was established, cell viability was studied to confirm that the bioink adequately supports cell survival and functionality over time. In addition, to enhance self-stability and further improve the shape fidelity of the 3D bioprinted construct, an *ad hoc* crosslinking process of alginate is developed. The bioink is designed with the need to culture the bioprinted construct for several weeks while preserving the support for embedded cells.

2. Materials and methods

2.1. Design of dECM-based bioink

Sodium alginate (MP Biomedicals, US), gelatin from bovine skin (Type B, Sigma-Aldrich, US), and dECM of porcine aorta were mixed at different ratios to find an optimal blend to ensure shape retaining after the extrusion process (S.I. 1). To obtain a sterile bioink, the powders of alginate and gelatin were disinfected in 100 % ethanol (Sigma-Aldrich, US) for 8 h. Porcine aortas of 6-month-old female and male pigs were kindly provided by a local abattoir, and the thickness of each sample was measured with a digital caliper. dECM was obtained according to a previously developed protocol [42]. Briefly, the steps of the decellularization protocol consisted of washing the samples in deionized water (dH_2O) for 1h, followed by 4h in 4 % (w/v) deoxycholic acid (Sigma-Aldrich, US) and 1h in dH_2O. The last step involved 3h in 22.5 mg/l DNase (Sigma-Aldrich, US) in 0.9 % (w/v) sodium chloride.

Subsequently, dECM powder was obtained by cryomilling under N_2. Then, the powder was enzymatically digested for 7 days with pepsin from porcine gastric mucosa (Sigma-Aldrich, US) according to the weight ratio 1:0.1 (dECM: pepsin). The enzyme was activated by the addition of HCl (Sigma-Aldrich, US) in a 0.8 % (w/v) NaCl solution, reaching a molarity of 0.01 [43]. At day 7, the enzymatic digestion of the dECM suspension was neutralized by adding dropwise 10M NaOH (Sigma-Aldrich, US) [44]. The concentration of the resulting digested porcine aorta dECM suspension was 1 % (w/v) and was used as solvent for alginate and gelatin powders. To produce the dECM-bioink, firstly gelatin was dissolved in digested dECM suspension under continuous stirring at 45 °C for about 15 min, and then alginate was added at 37 °C, keeping stirring. The range of final concentrations investigated varied from 1 % (w/v) to 7 % (w/v) for both alginate and gelatin (S.I. 1).

As a control, a water-based bioink composed of sodium alginate and gelatin (Alg-gel bioink) was produced adopting the above-mentioned protocol.

2.2. Double crosslinking process

A double-step crosslinking process was experimentally optimized to ensure shape fidelity during the printing process and the preservation of the printed structure over time (S.I. 1). This process involved a pre-printing internal crosslinking of sodium alginate through calcium carbonate ($CaCO_3$, Sigma-Aldrich, US) and glucono-δ-lactone (GDL, Sigma-Aldrich, US) [45], followed by a post-printing external crosslinking with calcium chloride dihydrate ($CaCl_2$, Sigma-Aldrich, US) solution [46]. $CaCO_3$ was sterilized by autoclave, while GDL and $CaCl_2$ solutions were syringe-filtered (filter diameter 0.22 mm). Different percentages of $CaCO_3$ ranging from 0 % (w/v) to 0.7 % (w/v) were evaluated during the experimental study (S.I. 1). After adding $CaCO_3$, the internal pre-printing crosslinking was triggered by adding GDL solution to the bioink with a double-syringe method. The percentages of GDL evaluated

during the optimization ranged from 0 % (w/v) to 2 % (w/v), and the internal crosslinking time ranged from 15 min to 24 h(S.I. 1). Finally, the second external crosslinking was performed immediately after the printing phase by soaking the construct in 1 % (w/v) $CaCl_2$ solution at 4 °C for a time ranging from 5 to 10 min.

2.3. Rheological tests

Viscoelastic properties of dECM-enriched bioink were evaluated by a modular rheometer (MCR 502e, Anton-Paar, AT). All rheological tests were performed in triplicates on two independent batches.

Frequency sweep tests were performed by adopting a double plate geometry with 25 mm diameter plates. For these tests, a strain amplitude of 0.5 % was set, and a logarithmic increase of frequency was set between 0.1 Hz and 20 Hz. Rheometer plates were heated up to 37 °C controlled with a Peltier plate, to better mimic the printing conditions, and the experimental environment was maintained humidified to avoid the drying of the samples. The gap between the two plates was set equal to 0.5 mm. From frequency sweep tests, the viscosity and shear rate values were derived from the torque, the plate radius and gap, and the angular frequency of the upper plate. The outcome of this test is a plot in which the viscosity is expressed as a function of the shear rate to evaluate the viscous properties of the tested bioink, and to understand if samples are characterized by a shear-thinning behavior.

To evaluate the internal crosslinking kinetics, storage modulus (G′) and loss modulus (G″) values were acquired for 65 min employing a cone-plate geometry with 50 mm diameter. Particularly, G' and G'' behaviors over internal crosslinking time were evaluated through time-sweep analyses at a fixed strain amplitude and frequency of 0.5 % and 1 Hz, respectively. The distance between the cone and the plate was equal to 0.1 mm. During time-sweep tests, the temperature was set at 37 °C, and the experimental environment was maintained humidified to avoid the drying of the samples.

2.4. Printability evaluation

A quantitative printability assessment on mono-layered structures was carried out by bioprinting fibers with a length of 30 mm and 20 mm × 20 mm square grids (grid infill density: 25 %) with a pneumatic 3D bioprinter Inkredible+ (Cellink, Sweden). The 3 ml cartridge (Cellink, Sweden) was equipped with a 22G conical nozzle (Cellink, Sweden) and a 10 mm/s printing speed was set. Pressure was manually increased to ensure a continuous flow of bioink. During printing, pressure was slightly increased due to the reactive cross-linking to ensure the filament extrusion. The printability of dECM-based bioink was assessed at the beginning (t = 0) and after 30 min of internal crosslinking. Printability of Alg-gel bioink was evaluated at the same conditions as control. Immediately after the printing step, filaments and grids' pores were imaged by an optical microscope (Eclipse Ti2, Nikon, Japan) at 4x of magnificence and analyzed with Fiji (Imagej) software.

The shape retaining of the bioprinted fibers was quantified by computing the Spreading Factor (S) as follows (Eq. (1)):

$$S = \frac{D_n}{D_f} \bullet 100 \tag{1}$$

where D_n is the diameter of the employed nozzle (0.41 mm), while D_f is the mean diameter computed on 30 random filament points. The value of spreading factor is expressed as the average measurements on three (n = 3) different filaments ± standard deviation.

The homogeneity of the printed coils was evaluated by calculating the Uniformity Coefficient (U), according to (Eq. (2)):

$$U = 1 - \frac{\sigma_{Df}}{D_f} \tag{2}$$

where σ_{Df} is the standard deviation of 30 fiber random diameters, while D_f is the same mean value used in Eq. (1) averaged on 30 random points. The uniformity coefficient is represented as the mean of measurements taken from three (n = 3) different coils ± standard deviation.

Pore coefficient (Pr) was computed to evaluate the shape fidelity of n = 5 random pores of a bioprinted grid, as follows (Eq. (3)) [47]:

$$Pr = \frac{(P)^2}{16\,A} \tag{3}$$

where P is the pore perimeter and A is the pore surface.

The perimeter coefficient (Pe) was calculated to evaluate the shape retention of the perimeter of the bioprinted grids as follows (Eq. (4)):

$$Pe = \frac{1}{\left\{\left[\frac{1}{2} \bullet \left(\frac{L_{bx}}{L_x} + \frac{L_{by}}{L_y}\right) - 1\right] + 1\right\} \bullet \left[1 + \frac{1}{2} \bullet \left(\frac{\sigma_{bx}}{L_x} + \frac{\sigma_{bx}}{L_y}\right)\right]} \tag{4}$$

where L_x and L_y are the lengths of CAD model sides, while L_{bx} and L_{by} are the average lengths of the printed sides parallel to the x- and y-axis, respectively. σ_{bx} and σ_{by} are standard deviations of bioprinted side lengths. The Perimeter coefficient was evaluated averaging n = 3 bioprinted grids and calculating standard deviation.

2.5. Model and 3D-bioprinting of multi-layered vessel

The pre-processing of 3D bioprinting of dECM-based multi-layered vessel involved the development of a customized printing code (GCode). The aorta CAD model was produced with Fusion 360 (Autodesk, US), and its dimensions were chosen according to those of the native aorta: 20 mm for the inner diameter and 2 mm for the wall thickness (Figure S. I.2(a)). By appropriately choosing the CAD model height equal to 8.2 mm or 16.4 mm, it was possible to obtain 20- or 40-layer constructs, respectively (Figure S.I.2(b)). Heartware (Cellink, Sweden) software was employed as slicing software to generate the GCode. The infill parameter was set as 'circular'. Two 3 ml cartridges (Cellink, Sweden), both supplied with 22G (0.41 mm) conical nozzles (Cellink, Sweden) were loaded on the bioprinter during the printing process. 3 ml of dECM-enriched bioink was split into two cartridges to print a 20-layer construct. For preliminary tests on printability, two dyes were used to distinguish between the vascular tunics. A blue dye was employed for the intimal and adventitial layers, while a green dye for the media layer (Figure S.I.2(c)). The printing speed was set at 10 mm/min, and the cartridge housing temperature was set at 37 °C. The same protocol was used to print the Alg-gel bioink.

For cell viability assays, the cell suspension was added to the bioink immediately after mixing the GDL solution, according to the ratio 1:0.1 at a density of 2×10^6 cells ml^{-1}. 20 and 40-layered constructs were obtained using the CAD model and the printing protocol previously mentioned. After printing, the cellularized constructs were externally crosslinked and routinely cultured in a complete growth medium at 37 °C, 5 % CO_2, and 95 % relative humidity.

2.6. Evaluation of shape fidelity

2.6.1. Filament drop test

A filament drop test was performed extruding through a 22G nozzle the dECM-based bioink immediately after the GDL addition, at 15, 30 and 45 min of internal crosslinking. To form a filament and to maintain a consistent filament diameter, the air pressure was adjusted based on the crosslinking time (0 min–10 kPa; 15 min–20 kPa; 30 min–45 kPa; 45 min–100 kPa). The filament uniformity at different degrees of internal crosslinking was observed using a camera and qualitatively analyzed.

2.6.2. Filament collapse test

The filament collapse test is based on the work of Therriault et al., 2007 [48] and Ribeiro et al., 2018 [49] where the mid-span deflection of a suspended bioink filament was analyzed. An ad-hoc structure featuring

pillars spaced at predefined gap distances (1.0, 2.0, 3.0, 4.0, 5.0, and 8.0 mm, Figure S.I.3 (a)) was designed and fabricated in poly lactic acid (PLA) using an FDM 3D printer (Kentstrapper, Florence, IT). A single filament of internal crosslinked dECM-based bioink was deposited across the gaps using a pneumatic 3D bioprinter Inkredible+ (Cellink, Sweden). More in detail, bioinks at different degrees of internal crosslinking were loaded into 3 ml syringe (Cellink, Sweden) and extruded through a 22G conical nozzle (Cellink, Sweden), imposing the pressures mentioned in section 2.6, with a deposition speed of 10 mm/s. The nozzle tip was positioned 0.1 mm above the top surface of the pillars, and the print path extended 5 mm beyond the last pillar. The filament deflection was measured immediately after printing by determining the deflection angle θ at the edge of the suspended filament using Fiji (Image J) software. The angle θ was plotted against the pillar distance 2L (Figure S.I.3(b)).

2.6.3. Filament fusion test

The filament fusion test involves printing a single-layer coil of parallel strands with progressively increasing spacing relative to the nozzle diameter (Figure S.I.4). To maintain a consistent filament diameter of around 0.41 mm across all samples, the deposition speed was set at 10 mm/s, and air pressure was adjusted according to each concentration as described in section 2.6. The bioink was extruded at 15, 30, and 45 min of internal crosslinking. Images were taken directly after printing using a microscope (Eclipse Ti2-E, Nikon, Japan, magnification ×4). The filament lengths were measured using Fiji (Image J) software, and the results were plotted for each crosslinking time point. To evaluate the effect of filament fusion at different degrees of crosslinking, the fused segment length (fs) was measured at various filament distances (fd) (Figure S.I.3). To account for variations in filament thickness (fw) among different crosslinked dECM-based gels, fs was normalized by dividing it by the average fw for each sample.

2.6.4. Shape fidelity of 3D bioprinted constructs

Shape fidelity of double-crosslinked aortic segments was evaluated on 20-layer constructs bioprinted with externally crosslinked dECM-bioink and with Alg-gel bioink, chosen as control. The height and the thickness of three (n = 3) constructs were measured through a digital calliper after crosslinking with 1 % (w/v) $CaCl_2$ at 4 °C for 10 min to assess the shape fidelity of the printed construct compared to the CAD model. To investigate the ability of the printed constructs to reproduce the native structure of the native aorta and their inter-sample variability, the wall thickness of three (n = 3) bioprinted vessels was compared to the thicknesses of three (n = 3) porcine aortas.

2.7. Swelling and degradation tests

To evaluate the weight variation of dECM-based constructs due to swelling, three (n = 3) 20-layer constructs were bioprinted, externally crosslinked with 1 % (w/v) $CaCl_2$ at 4 °C for 10 min and incubated at 37 °C in dH_2O supplemented with 1 % (v/v) Penicillin-Streptomycin. Then, three (n = 3) 20-layer constructs were soaked in a complete growth medium to mimic cell culture conditions. The weight variation was calculated by measuring the weight of each sample at specific time points, i.e., 15, 30 min, 1, 2, 3, and 5 h. The weight variation (ΔW) at each time point was calculated as in Eq. (5):

$$\Delta Weight\ (\%) = \frac{W_{timepoint} - W_0}{W_0} \times 100 \tag{5}$$

where $W_{timepoint}$ is the weight of the samples at each time point and W_0 is the weight of the samples before immersion.

At swelling equilibrium, the height and the wall thickness of the constructs were measured with a digital caliper and compared with the height and wall thickness before immersion to evaluate shape fidelity retention after swelling. Moreover, height and thickness of constructs swelled in DMEM were compared with those of the CAD model and the native aorta, respectively.

The test was repeated on Alg-gel constructs to understand the influence of dECM on swelling property.

To evaluate the degradation of dECM-enriched and Alg-gel constructs, three (n = 3) samples for each bioink formulation at swelling equilibrium were incubated at 37 °C in a complete growth medium and weighed at day 1, 4, 7, 14, 21 and 28. Weight variation due to degradation was computed as in Eq. (6):

$$Degradation\ rate\ (Dr\ \%) = = \frac{W_s - W_{timepoint}}{W_s} \times 100 \tag{6}$$

where W_s is the weight at swelling equilibrium.

At the end of the degradation test, sample dimensions were taken with Fiji (ImageJ) software to evaluate the shape retaining over time of bioprinted constructs under normoxic conditions. Wall thickness was compared with that of the native aorta, while the height with the CAD model one.

2.8. Cell culture

Mouse fibroblast cells (L929; Catalog No. CCL-1™, American Type Culture Collection, passage 10–11) were embedded in the dECM-based bioink to evaluate the cytocompatibility of the bioink and printing process. L929 cells were grown in a complete growth medium composed of high glucose Dulbecco's Modified Eagle's Medium (DMEM) supplemented with 10 % (v/v) fetal bovine serum (FBS) and 1 % (v/v) Penicillin-Streptomycin solution. The cells were cultured at 37 °C, 5 % CO_2, in a humidified environment.

2.9. Cell viability assay

Cell viability in five 3D-bioprinted constructs (n = 5) was evaluated at day 1 and 7, after the printing process, using a Live&Dead kit (Invitrogen, USA) according to the manufacturer's instructions. Briefly, the samples were washed in PBS and then incubated in a staining solution containing 0.5 μl ml^{-1} calcein-AM and 2 μl ml^{-1} of ethidium homodimer at 37 °C for 45 min. Then, samples were rinsed in PBS. Eclipse Ti2-E (Nikon, Japan) microscope was employed to acquire bright field and fluorescence images of live (green) and dead (red) cells within the printed constructs. Images were analyzed using Fiji (Image J) software.

2.10. Uniaxial tensile tests

To test mechanical properties of the 3D bioprinted constructs with dECM-based, n = 3 ring shaped specimens with a height (H) of 5 mm were bioprinted and mounted onto suitable holders (Fig. 1) on a electromechanical testing machine (MTS Synergie200H, Eden Prairie, MN) equipped with a 100 N load cell. Initial sample length was defined as the distance between grips when a reference pre-load of 0.015 N was applied. For the measurement of the printed samples dimensions, ImageJ software was used to avoid damaging the construct with caliper. The considered measurements included the height (H) and thickness (S) and were calculated averaging five measurements per sample. Each sample was subjected to tensile test with two cyclic loadings, with a speed of 10 mm/min and load endpoint of 0.4 N. At the end of the tests the tensile stress σ (MPa) and the percentage length variation ξ were calculated as follows (Eq. (7), Eq. (8))

$$\sigma = \frac{F}{2*H*S} \tag{7}$$

$$x = \frac{\Delta L}{L_0} \tag{8}$$

Where ΔL is the grip separation, F is the measured force, and L_0 is the

Fig. 1. Tensile test set-up for holding the 3D bioprinted multilayered vessels.

gauge length at 0.015N of load. Particularly, the residual elongation was calculated as the zero-force deformation of the last cycle. The ring stiffness E(Pa) represents the slope of the stress-strain curve in the elastic region. It is defined as the ratio of stress σ to percentage length variation x.

2.11. Statistical analyses

Statistical analyses were performed using Word Excel (Microsoft Corporation, USA). Results are presented as mean ± standard deviation. Standard deviations are displayed as a bar in graphs. Unpaired *t*-tests were used to compare two independent groups of data. If the *p-value was higher than 0.05* ($p > 0.05$), data were considered not significantly different (NS), while if the *p-value was lower than 0.05* *($p < 0.05$) data were considered statistically different.

3. Results

The development of the bioink involved an optimization phase, during which the role of $CaCO_3$ in regulating the availability of Ca^{++} ions for cross-linking was carefully considered. To determine the optimal concentration of the dECM-based bioink, experiments that included the 3D printing of basic structures such as grids and coils were conducted. Subsequently, 3D bioprinted constructs were comprehensively characterized evaluating their rheological properties, swelling, and degradation behaviors, as well as monitoring cellular viability over time. This characterization encompassed both cellular and structural aspects.

3.1. Optimization of the bioink composition and bioprinting process

The optimization of the bioink was performed by considering the influence of $CaCO_3$ on the availability of Ca^{++} for crosslinking. It was hypothesized that the quantity of $CaCO_3$ directly regulates the degree of crosslinking, thereby promoting the transition of a viscous solution into a solid gel. However, the Ca^{++} is only available upon acidification by the time-dependent hydrolysis of the lacton ring of GDL, as the acidification promotes the dissolution of $CaCO_3$. Therefore, the amount of $CaCO_3$ was refined to tune the extent of the crosslinking and GDL to control the kinetic of the crosslinking. The time-dependent gelation controlled by the internal crosslinking was further associated with a second gelation induced by the $CaCl_2$ (external gelation). This fine-tuning of the crosslinking degree and rate was essential to generate self-supporting structures during and after the printing process, capable of withstanding the load exerted by subsequent layers. The experimental optimization of alginate double-crosslinking resulted in a 30-min internal pre-printing crosslinking with 1.2 % (w/v) GDL and 0.5 % (w/v) $CaCO_3$ as final concentrations and in a 10-min external post-printing crosslinking soaking constructs in a 1 % (w/v) $CaCl_2$ solution for 10 min.

The optimal concentration of the dECM-based bioink was identified through preliminary tests on the shape fidelity of printed simple structures, such as grids and coils. Since alginate enhanced flexibility and structural stability, its final concentration was maximized. Conversely, gelatin provides initial stability to the segment [21] but also leads to the embrittlement of the bioink. Therefore, we minimize its quantity in the bioink accordingly. 1.2 % (w/v) gelatin and 6 % (w/v) sodium alginate formulation were found as the best compromise between printability and shape fidelity. The resulting concentration of dECM was 0.66 % (w/v).

The optimization process was followed with the rheological characterization of the final composition. The first aspect to be tested was the kinetic of the crosslinking as it controls the extrudability of the hydrogel during the printing process.

3.2. Rheological characterization

As proof of concept that our bioink was capable of self-supporting high-z structures, with defined and confined layers, rheological tests were performed on the dECM-bioink. Frequency sweep analyses revealed an increase in both the conservative (G') and loss (G″) moduli when the ink was additionally crosslinked with $CaCl_2$-based external gelation (Fig. 2(a)). The values of G′ sampled at the frequency of 1.05 Hz of the not-crosslinked, internally crosslinked and double crosslinked bioinks, showed the possibility to exponentially increase G′ with the double crosslinking approach (Fig. 2(b)). Specifically, the value of G′ increased of 0.86 kPa after 30 min of internal crosslinking. Finally, the post-printing treatment with $CaCl_2$ increased G′ of 4.5 kPa. In Fig. 2(c), G′ and G" are plotted over the reaction time to evaluate the kinetics of the internal crosslinking to identify the printability window. The crossover point of G′ and G″ is identified at 11.2 ± 0.76 min (n = 3). This point indicates the moment from which the viscoelastic behaviour of the material switches from liquid-like to solid-like. This result is echoed by the trend of the loss factor tan(δ), represented in Fig. 2(d). This graph also highlights that after 30 min from the beginning of the internal crosslinking, the kinetics of the loss factor reach a plateau, implying that from this moment the viscoelastic behavior of the ink should be sufficiently stable to allow reproducible printings. To preliminarily evaluate the suitability of ink to be extruded from a printing cartridge, a flow curve was measured after 30 min from the beginning of internal gelation. The viscosity (η) was evaluated at increasing shear rate values ($\dot{\gamma}$). Generally, the concept of viscosity is related to materials characterized by a liquid-like behavior (G'' > G′). Conversely, measuring it for solid-like materials (G' > G″) represents a conceptual mistake, since solids are not characterized by the ability to flow. Despite this, such a test can be adopted to provide information related to the rheological behavior of the ink rather than from measuring its viscosity. In this specific case (Fig. 2(e)), the bioink showed a shear thinning behavior characterized by decreasing values of the measured viscosity at increasing shear rates. This behavior enables the extrudability of the material while printing.

3.3. Quantitative and qualitative evaluation of shape fidelity

3.3.1. Filament drop test

The viscoelastic properties and crosslinking degree in a hydrogel are closely tied to its extrudability. Three distinct behaviors were observed during material extrusion at the minimum pressure, depending on the specific crosslinking time point. When not crosslinked, the bioink viscosity was too low, leading to accumulation at the nozzle and droplet formation (Fig. 3(a)); at this stage, the bioink could not print stable 3D

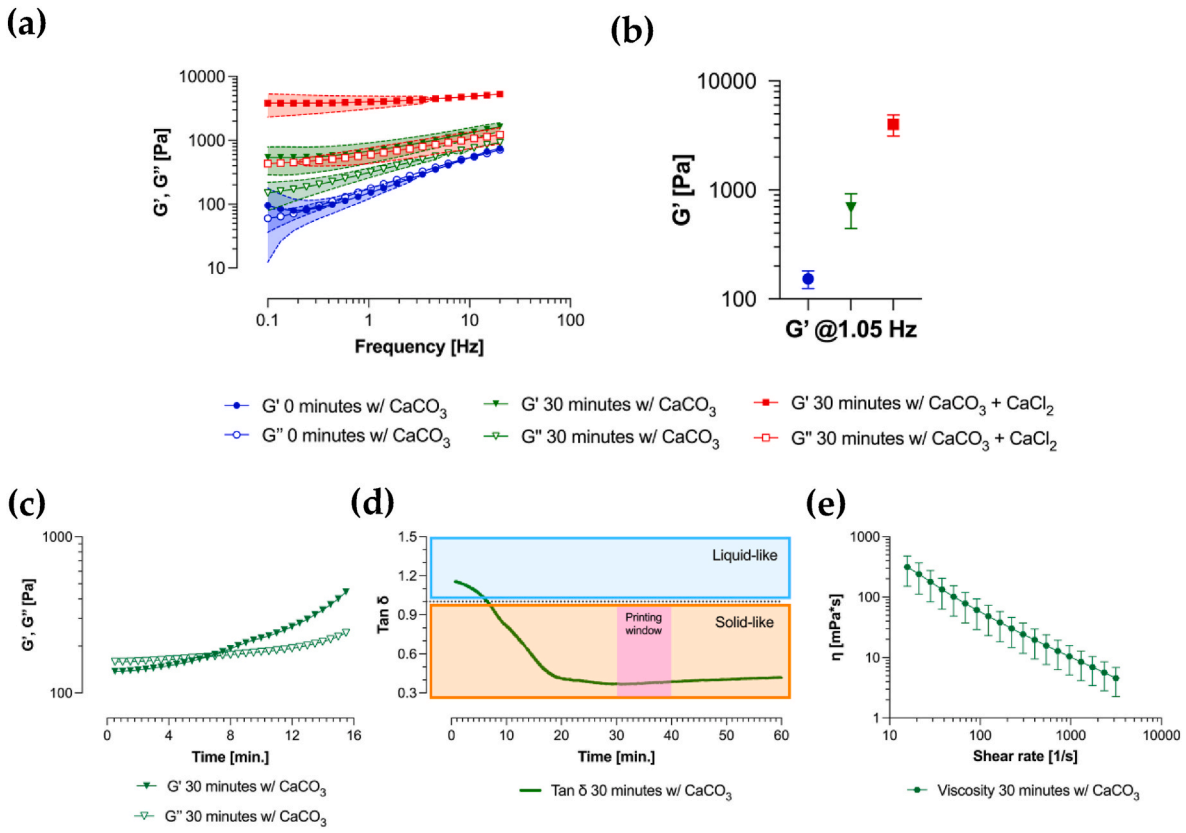

Fig. 2. (a) The conservative and loss modulus G′ and G″ plotted as a function of the frequency, depending on the crosslinking condition. (b) Values of the conservative modulus G′ sampled at the frequency of 1.05 Hz; this picture highlights the exponential increase of the conservative modulus between the beginning of the first crosslinking process (internal gelation) and the end of the second one (external gelation). (c) The conservative and loss modulus G′ and G″ measured as a function of the time at the frequency of 1 Hz provide insight into the crosslinking kinetics of the material and allow us to identify the gel point. Multiple analyses (n > 3) that were performed on these types of material suggest that variability of ±10 % should be considered both on G'and G". (d) The time-dependent trend of the loss-factor tan δ echoes results in panel (c). For the sake of clarity, the printing window identified for the proposed material is also highlighted in this chart. (e) The flow curve of the material highlights a decrease in viscosity as a function of the shear rate. This result highlights the shear-thinning behavior of the hydrogel.

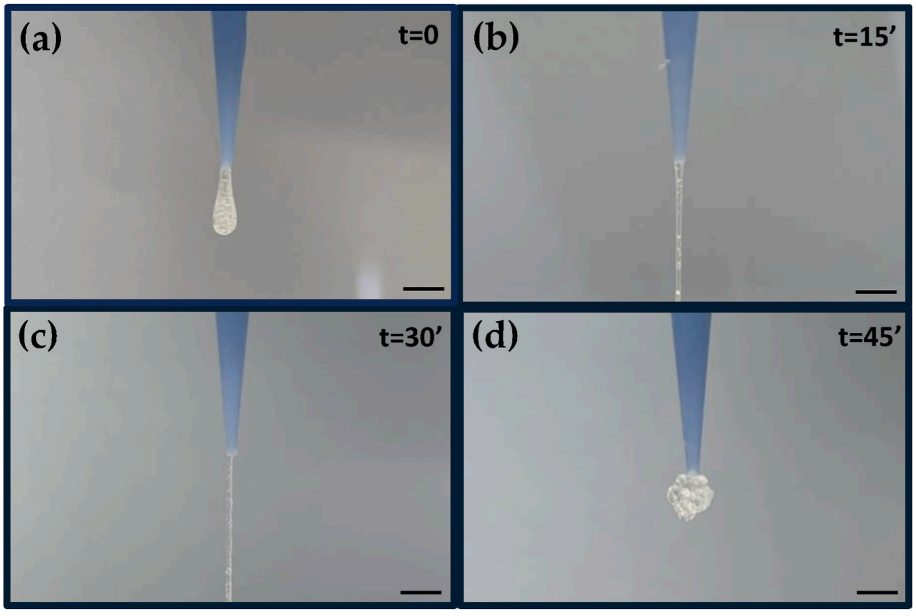

Fig. 3. Filament drop test of dECM-based bioink (a) not crosslinked, at (b) 15, (c) 30 and (d) 45 min of internal crosslinking. to the bioink. Scale bar: 2 mm.

structures. On the contrary, the hydrogels produced straight fibres (Fig. 3(b and c)) 15 and 30 min after GDL addition. While the dECM-bioink resulted in curly, non-straight filaments (Fig. 3(d)) at 45 min after GDL addition. At the 15-min time point, the gel generated short, discontinuous fibres with droplet-like material accumulation at the fibre ends. After 30 min, the filaments was straight and continuous, suitable for 3D bioprinting.

3.3.2. Filament collapse test

During the filament collapse test, the dECM-based bioink immediately after GDL addition and at 15 min of internal crosslinking was unable to produce stable filaments. Indeed, the bioink deposited on the PLA structure remained attached to the pillars (Fig. 4(a and b)). However, after 30 and 45 min of internal crosslinking, stable filaments were formed and suspended between the pillars (Fig. 4(c and d)), allowing for deflection angle measurements. Filament collapse increased with larger gap lengths, as shown by a greater deflection angle (θ) in Fig. 4(e).

3.3.3. Filament fusion test

Fig. 5 illustrates that the fs/fw ratio generally decreased, approaching the ideal unitary value as the distance between loops (fd) increased, resulting in a more uniform filament within the loop. With increased crosslinking time, the bioprinted ink was able to maintain distinct filaments at shorter distances compared to the bioink with a shorter crosslinking time (15 min).

3.3.4. Printability evaluation

Quantitative microscopic analyses of printability and shape retention after the bioprinting process were conducted. The first 30-min internal crosslinking step with GDL was effective in ensuring shape fidelity and retaining of the dECM-bioink. From the microscopic images of the extruded filaments, a difference in the spreading ratio between crosslinked (Fig. 6(b)(d)) and non-crosslinked (Fig. 6(a)(c)) filaments was noted. For the dECM-bioink, the spreading factor increased from 36.35 % ± 2.03–61.56 % ± 4.66, while for the alginate and gelatin-based bioink used as control, the spreading factor increased from 29.78 % ± 1.94–53.18 % ± 1.91 (Fig. 6(e)). The uniformity of the extruded

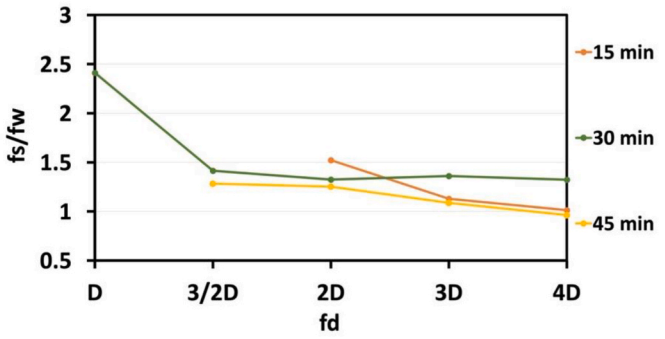

Fig. 5. Trend of the ratio between the filament diameter (fw) and the one at the loop peak (fs) in relation with the filament distance (fd).

filament, as the crosslinking occurred in both bioinks, decreased. The uniformity factor of the non-crosslinked dECM bioink displayed a value of 0.97 ± 0.008, while the crosslinked one showed a uniformity coefficient of 0.93 ± 0.014. The Alg-gel bioink also showed a slight decrease of the uniformity coefficient from the non-crosslinked bioink (0.95 ± 0.01) to the crosslinked one (0.90 ± 0.02) (Fig. 6(f)).

Grids bioprinted with non-crosslinked gels did not show hollow pores (Fig. 6(g)(i)), while at 30 min of internal crosslinking highly defined grids were 3D bioprinted with both dECM-based and Alg-gel bioinks (Fig. 6(h)(l)). Particularly, the pore coefficient from the grids bioprinted with the Alg-gel bioink displayed a value of 1.38 ± 0.17, while the pore coefficient of the dECM bioink was close to the ideal unitary value, specifically 1.15 ± 0.06 (Fig. 6(m)).

Finally, the perimeter coefficient was calculated from grids 3D bioprinted with crosslinked and pristine dECM-based (Fig. 6(i)(l)) and Alg-gel based hydrogels (Fig. 6(g)(h)). The 30-min crosslinked dECM-based bioink showed the best value of perimeter coefficient of 1.01 ± 0.01 (Fig. 6(n)).

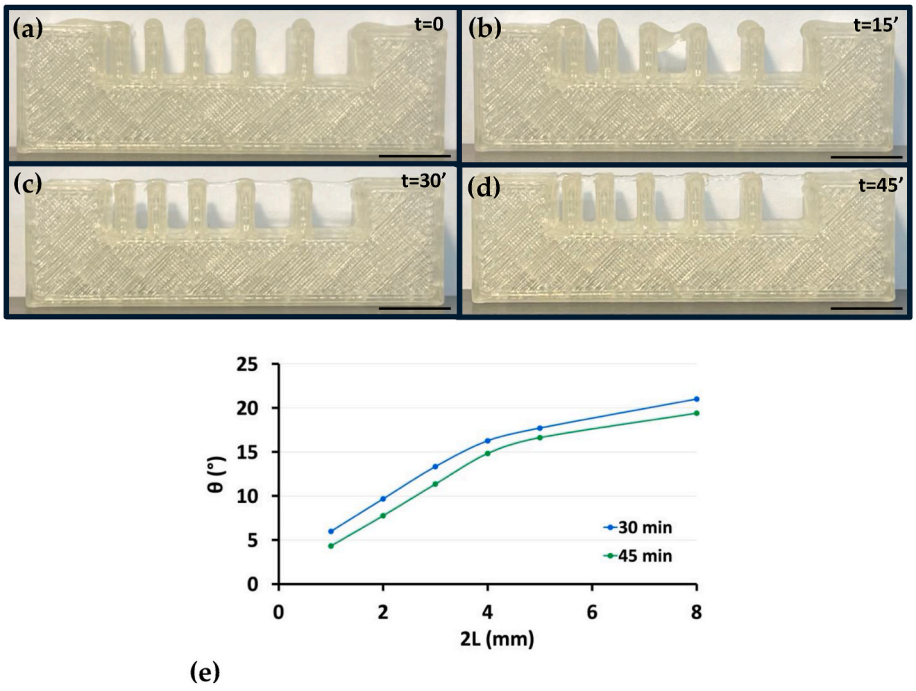

Fig. 4. Filament collapse test of dECM-based bioink (a) not crosslinked, at (b) 15, (c) 30 and (d) 45 min of internal crosslinking (e) Angle of deflection θ, in degree, as a function of the gap distance 2L, in mm.Scale bar: 5 mm.

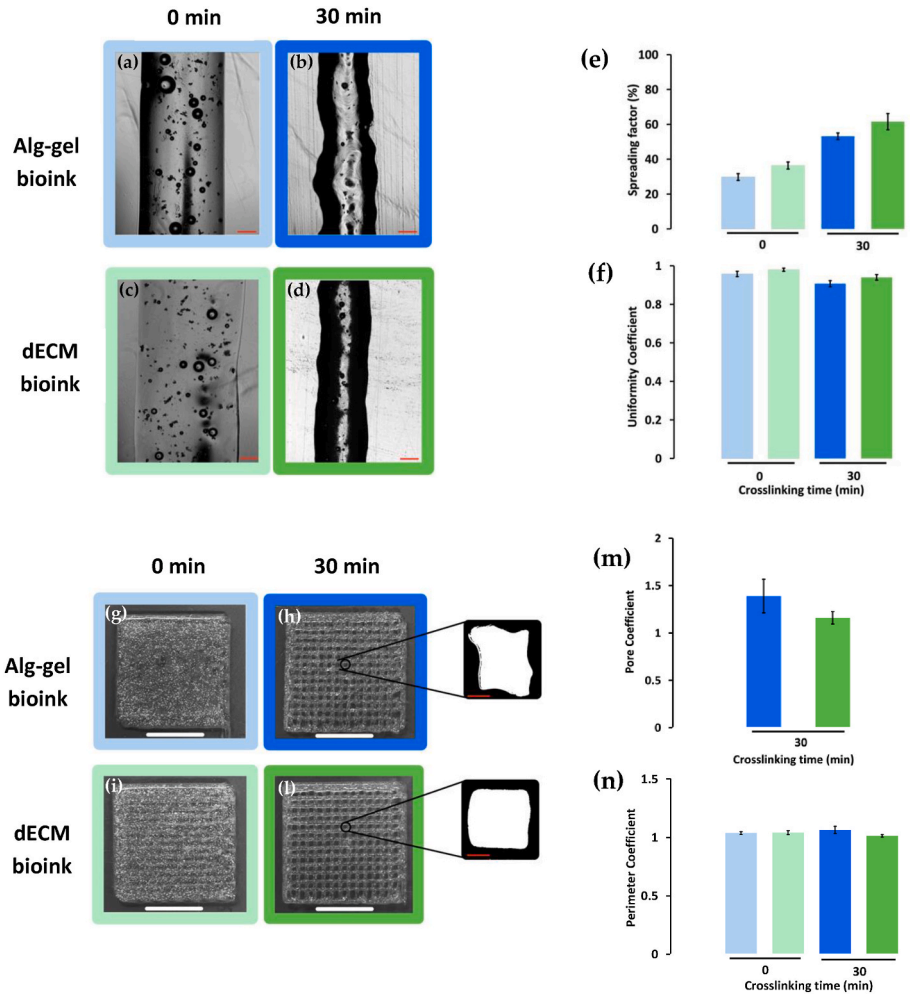

Fig. 6. (a) Not crosslinked and (b) crosslinked filament of alg-gel bioink. (c) Not crosslinked and (d) crosslinked filament of dECM bioink (Scale bar: 250 μm). (e) Spreading factor of not crosslinked and crosslinked Alg-gel and dECM bioinks (f) Uniformity coefficient of not crosslinked and crosslinked alg-gel and dECM bioinks. (g) Not crosslinked and (h) crosslinked grid of Alg-gel bioink (with pore magnification (4x), 250 μm) (Scale bar: 1 cm). (i) Not crosslinked and (l) crosslinked grid of dECM bioink (with pore magnification (4x), Scale bar: 250 μm) (Scale bar: 1 cm). (m) Pore coefficient of crosslinked Alg-gel and dECM bioinks. (n) Perimeter coefficient of not crosslinked and crosslinked Alg-gel and dECM bioinks.

3.4. Bioprinting of aortic-like constructs

During the bioprinting step, the pressure was gradually increased. The value of 40 kPa ensured a continuous filament of the dECM-based bioink with the final concentrations previously optimized and internally crosslinked for 30 min. Tubular structures were successfully printed up to 40 layers maintaining the shape during the bioprinting process (Fig. 7(a)) and after the post-printing crosslinking steps (Fig. 7 (b)(c)(d)). Indeed, during and after printing, no collapsing or overlapping of different vascular tunicae were observed (Fig. 7(e)(f)). The control bioink (Alg-gel), not containing ECM (composed of 6 % (w/v) sodium alginate and 1.2 % (w/v) gelatine) and internally pre-crosslinked for 30 min, needed a higher printing pressure (90 kPa) to obtain a continuous filament. The wall thickness (Fig. 8(a)) and the height (Fig. 8(b)) of the dECM-based bioprinted constructs were not statistically different from the height and wall thickness of the CAD model and the native aorta, respectively. Finally, there were no statistical differences between the dimensions of constructs bioprinted with dECM-based and Alg-gel hydrogels.

To further confirm their shape fidelity, the constructs based on dECM-enriched bioink were subjected to cyclic manual solicitation demonstrating the ability to resume their initial shape (See Supplementary materials).

3.5. Swelling and degradation behaviors

The weight of both hydrogels immersed in water significantly increased within the first hour up to about 53 % and 57 % for dECM-based bioink and Alg-gel bioink, respectively. Samples bioprinted with dECM bioink reached the swelling plateau after 3 h with a total weight increase of 54 %, while alginate-gelatin constructs were characterized by a weight increase of 57 % (Fig. 9(a)).

When submerged in a complete medium, similar swelling behaviors were noticed for the tested samples. In this case, swelling equilibrium was reached after 5 h and 3 h for dECM-based and alginate-gelatin bioink, respectively. At the swelling plateau, alginate-gelatin samples showed a weight increase of 35 %, while the constructs printed with dECM bioink showed a weight increase of 54 % (Fig. 9(b)). Fig. 9(c) shows no significant difference between the wall thickness of bioprinted segments at the swelling plateau and the one of the native aorta. Due to the major DMEM uptake by dECM-based vessels, the height of dECM-bioink-based vessels is different from that of the CAD model (Fig. 9 (d)). Because of DMEM absorption, wall thickness (Fig. 9(e)) and height (Fig. 9(f)) of dECM-based vessels, evaluated before and after swelling displayed different dimensions.

Fig. 10(a) reports the outcomes of the degradation rate (Dr) of dECM-based and Alg-gel constructs. A degradation test was conducted on

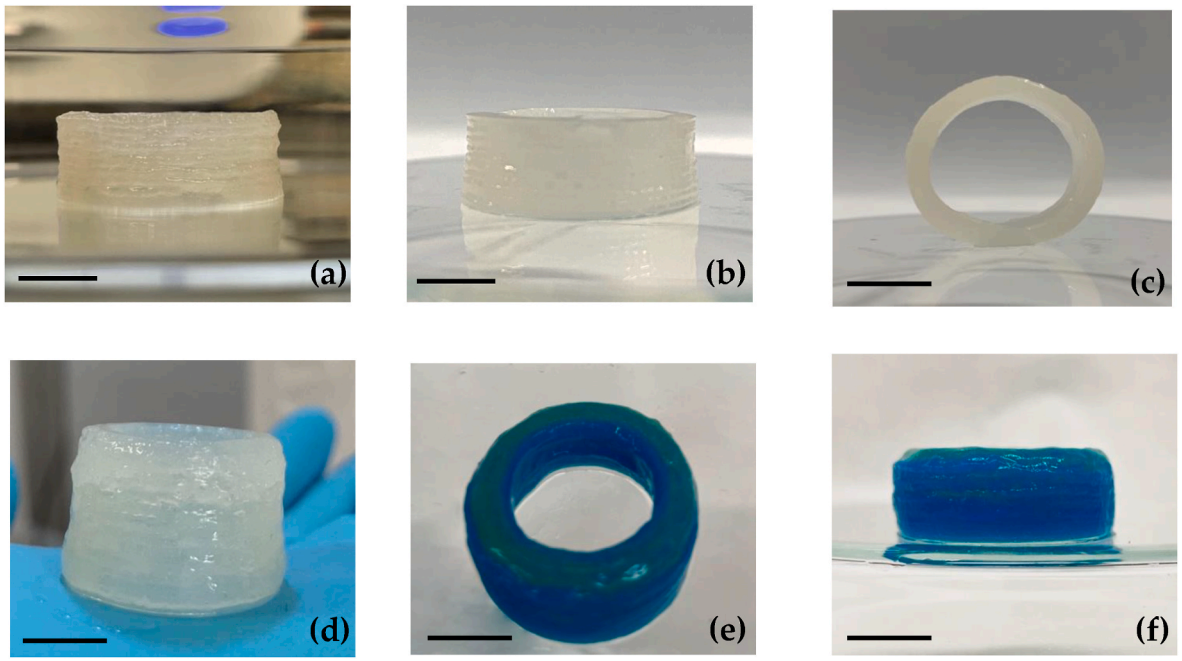

Fig. 7. (a) Front view of a 20-layer bioprinted vessel with dECM bioink after printing. (b,c) 20-layers bioprinted vessel with dECM bioink after external crosslinking with 1 % (w/v) $CaCl_2$ solution. (d) 40-layer vessel after double crosslinking. (e,f) Simulation of different cells deposition with bioink dyed. Scale bar = 1 cm.

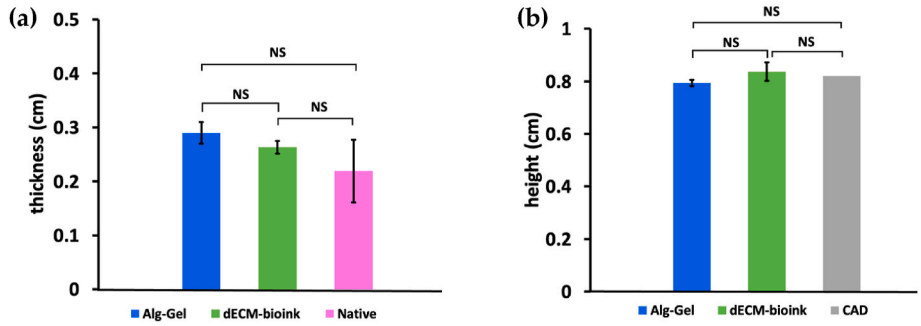

Fig. 8. (a) Comparison between the bioprinted vessels' wall thickness at the end of the post-printing crosslinking and that of the native porcine aorta. (b) Evaluation of aortic segments' height after the post-printing crosslinking with respect to that of the CAD model.

samples at the swelling plateau (Fig. 10(b)). After 28 days (Fig. 10(c)) the mean weight of vessels bioprinted with dECM bioink was 87 % of the initial weight. On the other hand, the degradation test of alginate-gelatin bioink stopped at 26 days of incubation due to structural failure, at that time, the percentage of the initial weight was 87 %.

After 28 days the wall thickness (Fig. 10(d)) and height (Fig. 10(e)) of the aortic constructs bioprinted with dECM-bioink did not show statistical difference when compared to the one of the native aorta and CAD model, respectively, thus confirming that the bioprinted constructs maintained their structural stability over time.

3.6. Cell viability assay

Cells were mostly alive after 24 h from the bioprinting phase (Fig. 11 (a)), thus indicating that the bioprinting process, including the pre-printing crosslinking, extrusion, and post-printing crosslinking, did not affect cell viability. Moreover, cell viability 7 days after printing (Fig. 11 (b)) confirmed that the dECM biomaterial ink is suitable to support 3D cell culture. From the images, it seems that cell number increased over time from day 14 (Figure S.I. 5(a)) up to day 21 (Figure S.I. 5(b)). From day 14 to day 28 (Figure S.I. 5(c)) is appreciable the enhancement of cell adhesion on the dECM-based bioink.

3.7. Uniaxial tensile test

The constructs were evaluated immediately after printing through uniaxial tensile tests, with cyclic loadings (Fig. 12(a) and (b)). As shown in Fig. 12 (c), the residual deformation (8.3 ± 1.2 %) and the hysteresis area suggest the presence of energy dissipating phenomena. The second cycle resulted in a reduction of the hysteresis area. The measured ring stiffness was 31.1 ± 1.7 kPa, calculated in the linear region of the first loading cycle. The initial length L_0 (Fig. 12 (a)) and the deformed length L_1 (Fig. 12 (b)) represent the specimen's elongation under load. Here, L_1 corresponds to the percentage length variation $\xi = 25$ %, indicating the relative length variation of the ring during testing Fig. 12 (c).

4. Discussion

3D bioprinting of cellularized vascular grafts presents a promising alternative to currently limited strategies. This technique holds great potential for the biofabrication of 3D cellularized constructs mimicking the hierarchical structure of vascular tissue [8,18,19].

The precise spatial organization of multiple cell types within distinct layers is critical for regenerating the hierarchical architecture of native tissues and promoting essential cell-cell interactions and paracrine

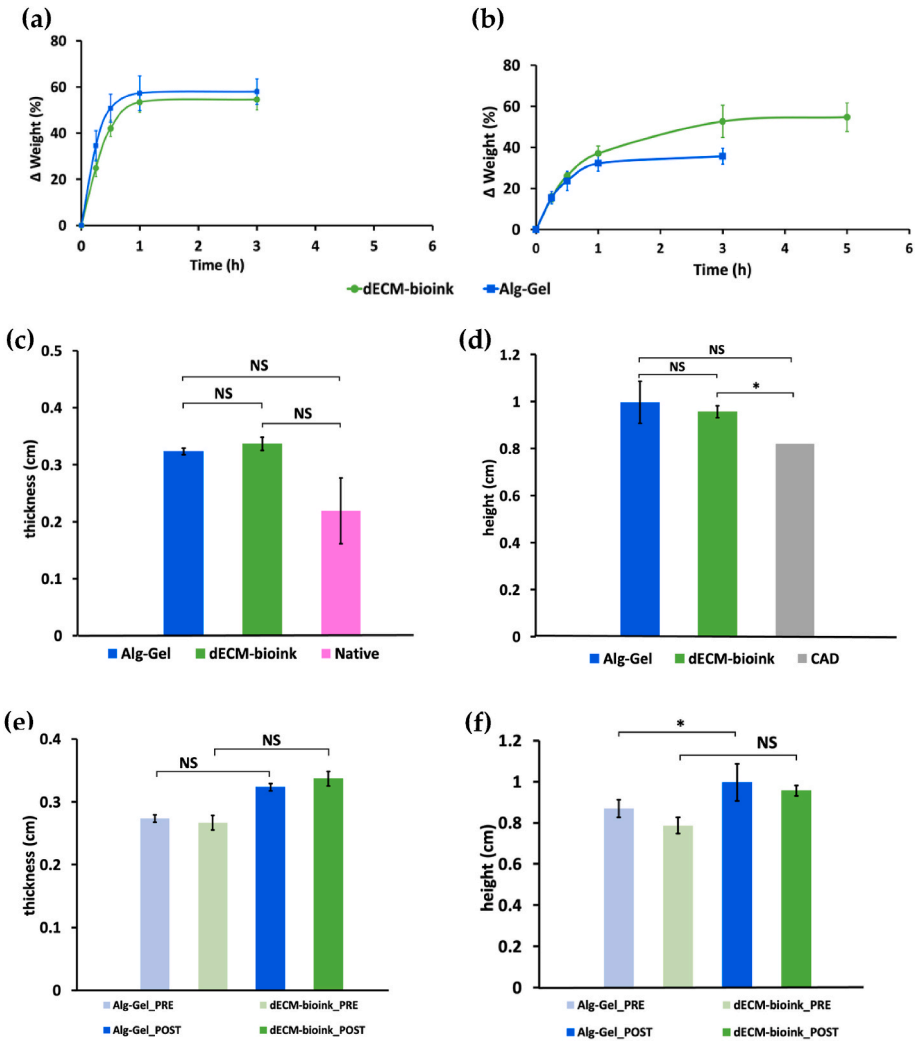

Fig. 9. Swelling behavior in dH_2O (a) and DMEM (b) of 20-layer vessels (n = 3) bioprinted with dECM bioink (green) and with alginate-gelatin bioink (blue). (c) Histogram with the comparison between the wall thickness dimensions of DMEM-swelled bioprinted vessels and the native aorta. (d) Comparison between the height of bioprinted vessels after swelling in DMEM and the CAD dimension (d). Evaluation of wall thickness (e) and height variation (f) before and after swelling in DMEM. (For interpretation of the references to colour in this figure legend, the reader is referred to the Web version of this article.)

signaling. Several studies have investigated bioprinting techniques to produce tubular constructs suitable for small vessels. However, despite progress, creating self-supporting tubular structures that closely mimic native vessel architecture remains challenging. As the focus shifts from bioprinting small vessels to fabricating anatomically relevant arteries, the scarcity of effective solutions becomes evident. A significant challenge in scaling up bioprinting for large vessels is maintaining cell functionality throughout the extended extrusion printing process. To tackle this challenge, a bioink capable of producing constructs with high shape fidelity and long-term structural stability while providing the necessary chemo-mechanical environment is required.

In this study, we developed a novel bioink able to provide the essential biochemical cues, by adding decellularized ECM, and to produce a self-sustaining and stable structure with relevant native-like dimensions thanks to an *ad hoc* crosslinking method of alginate. Thus, the biochemical signals, which are present in the native ECM and are vital to promote cell proliferation and differentiation, are included in the bioink [39–41,50,51,52]. There have been many attempts to introduce ECM into the material to replicate the native cellular environment of the liver [53,54], cartilage [55], or cardiac tissue [12], for example. The alginate-gelatin matrix was the key to control the crosslinking kinetics and the final rheological properties of the bioink, as lyophilized ECM loses its native mechanical characteristics upon extraction and enzymatic digestion [43,56].

Synthetic-based cell-loaded hydrogels for blood vessel construction [36] were previously produced with PEGDA and GelMA. Despite their capability to achieve favourable shape fidelity and printability, enabling the creation of substantial constructs, they do not include the biochemical signals and the mechanical microenvironment of native tissues. Tubular constructs were produced with a polysaccharide-based bioink with no biochemical cues included in the natural derived hydrogel [33].

The bioprinting process was optimized by the tight control of the crosslinking process, thanks to the rheological tests. Two different steps of crosslinking were considered. The first step is based on reactive printing by the control of the internal gelation [45]. The principle is to optimize a printability window during the crosslinking process. In this specific case, the identified printability window corresponded to about 30 min after triggering the internal crosslinking (Fig. 2(d)). This expands the possibilities of the 3D bioprinting process, as the reactive crosslinking enabled the constructs to support their weight even when printing the 20 or 40 layers (corresponding to 20 mm) (Fig. 7 (b)(d)). This result goes far beyond what was previously achieved without the aid of any support. Internal gelation was previously reported as a pre-crosslinking method, but the final stabilization was based on external gelation [46].

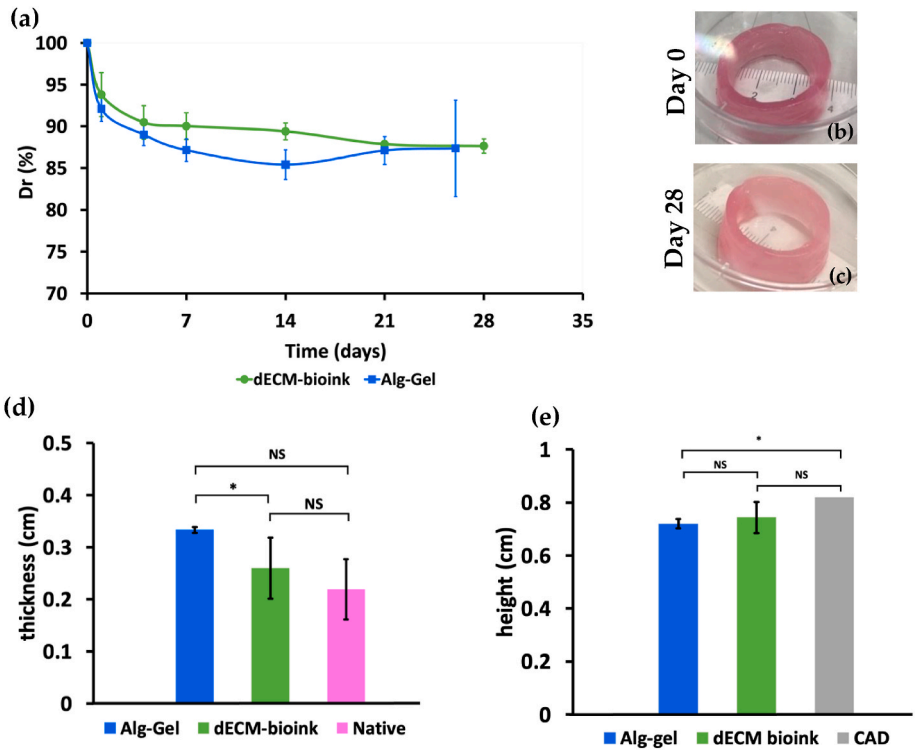

Fig. 10. (a) Degradation Rate (Dr) of 20-layer vessels bioprinted with dECM-bioink (green) and with alginate-gelatin bioink (blue). (b) 20-layer vessel bioprinted with dECM-bioink at swelling equilibrium (c) and after 28 days of incubation in DMEM. (d) Comparison between the bioprinted vessels' wall thickness at the end of the degradation test and that of the native porcine aorta. (e) Evaluation of aortic segments' height at the end of the degradation test with respect to that of the CAD model. (For interpretation of the references to colour in this figure legend, the reader is referred to the Web version of this article.)

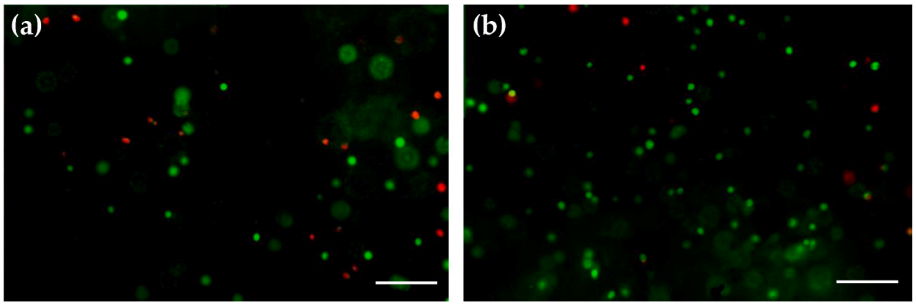

Fig. 11. (a) Live&Dead staining images acquired at 24 h and at 7 days (b) of static culture. Images taken under optical microscope at 14 days (c), 21 days (d) and 28 days (e). Scale bar: 100 μm.

Tan and co-workers [33] 3D bioprinted a vascular segment of about 2 cm with an alginate-xantan gum hydrogel, without any external support. However, the external crosslinking performed with a $CaCl_2$ solution caused the shrinkage of the printed hydrogel compromising the resolution of the tubular structure.

In our case, the external post-printing crosslinking gives the construct toughness and stability over time (Fig. 11(c)), maintaining the designed dimensions and pushing further what was previously done for a construct of a height of about 5 mm, where snap-stabilization of the final structure was required for minimizing the time interval from bioprinting to culture [54]. The double-crosslinking process increased exponentially G′, as shown by the interpolation plot of the three values of G' in Fig. 2(a). Moreover, thanks to this double-crosslinking process, the constructs demonstrate a ring stiffness of 31.1 kPa, allowing for easy handling and the ability to recover 90 % of their original shape, even after being exposed to cyclic stresses. The preliminary biological characterization of the bioink, conducted by embedding a fibroblast cell line in the dECM bioink, proved that cells were alive 1 and 7 days after printing, thus opening the way to the use of this material for tissue engineering. Initial assessments showed that the majority of cells remained viable 24 h post-bioprinting (Fig. 11(a)), indicating that the entire bioprinting process—including pre-printing crosslinking, extrusion, and post-printing crosslinking—did not negatively impact cell viability. Further analysis revealed sustained cell viability 7 days after printing (Fig. 11(b)). The anatomy of the large blood vessel wall is composed of three tunicae: the tunica intima, consisting of a thin monolayer of endothelial cells, the tunica media, the thicker tunica because predominantly composed of smooth muscle cells (up to 12 layers), and the tunica adventitia, primarily comprising fibroblasts.

Thanks to these excellent results, the next steps involve incorporating the three types of cells necessary to replicate the anatomical structure of the aorta. Specifically, we will focus on integrating endothelial cells, smooth muscle cells, and fibroblasts, with the goal of recreating the three distinct tunics of the aorta. This advanced phase of the project will bring us closer to developing a vascular model that faithfully mirrors the morphology and functionality of a native artery, paving the

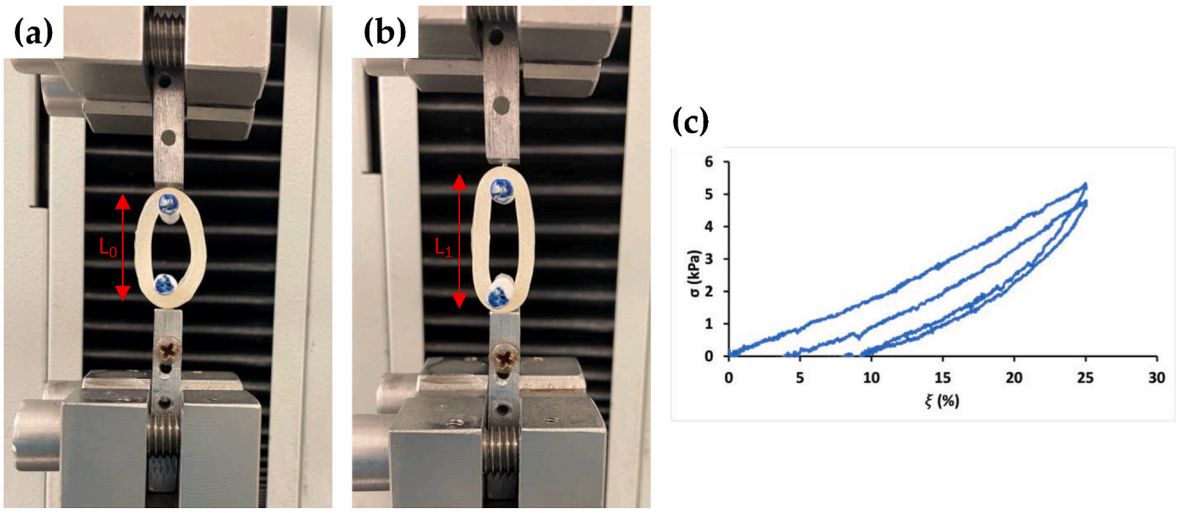

Fig. 12. Mechanical test setup showing the 3D bioprinted construct before (a) and after (b) deformation under cyclic load. The change in length from L_0 to L_1 highlights the elongation of the material under stress. (c) Cyclic tensile tests performed at velocity of 10 mm/min on 3D bioprinted constructs.

way for new clinical and research applications [57,58].

The 3D bioprinting technique enabled the replica of such a complex anatomical structure. Three layered-tubular constructs were previously bioprinted using Pluronic F127 as biocompatible ink [59]. Leveraging the capabilities of 3D bioprinting, it was possible to bioprint the three tunicae with an ECM-containing bioink, thus combining the control of the geometry with the control of the chemistry. The thickness variation for each tunica was successfully reproduced employing dyed bioinks (Fig. 7(e)(f)). The printing performed with dyed bioinks also demonstrated that the tunicae do not overlap during the printing phase. This important achievement is related to the double-crosslinking process optimized and opened the future development of bioprinting vessels with multiple cell types reproducing the different layers of the tunicae.

Several studies demonstrated that the degradation and the subsequential tissue regeneration process are influenced by numerous parameters such as biomaterial compositions and geometry [60,61]. For this reason, degradation tests have been performed on constructs with an aortic-like structure, to replicate real structural conditions.

The optimization of bioink formulation allowed the bioprinted vessels to reach the thickness of the native aorta and to preserve its shape over 28 days (Fig. 10(c)). Considering the structure composed of a degradable component such as gelatin, it can be hypothesized that due to the porosity generated by the degradation/dissolution of gelatin within the construct, vascularization may be promoted, which is fundamental to the formation of a living construct. On the other side, the stability induced by the presence of alginate allows for the handling of the construct and prolonged support for cell growth. Moreover, the slow degradation allows to culture the cellularized constructs first statically to allow cell stabilization, and then dynamically in a bioreactor to promote cell proliferation, infiltration, and tissue formation. Bioreactor conditions such as flow rates, shear stress, and pressure are essential for mimicking in vivo environments and promoting the maturation of biofabricated constructs [62]. Shear stress plays a key role in the formation of endothelial barrier, encouraging cell alignment, improving mechanical properties like elasticity and strength, and stimulating the release of bioactive substances that support vascular health. Pulsatile flow and rotational movement within the bioreactor ensure uniform nutrient distribution and oxygenation, fostering tissue remodeling and maturation [63–65]. Studies emphasize that optimizing these conditions is critical for developing functional, mechanically robust tissue-engineered constructs. Bono et al. designed a dual-mode bioreactor for fabricating and dynamically stimulating vascular constructs. The system cyclically inflates and deflates the support mandrel using sterile PBS, with a monitoring system controlling flow rate, pump direction, and switching between steady and pulsatile stimulation. According to their results, the mechanical conditioning enhanced gel compaction, matrix reorganization, and construct strength, as confirmed by mechanical tests [66]. Moreover, Pennings et al. developed a bioreactor system for culturing bi-layered vascular grafts under shear stress, with compartmentalized exposure of the graft's luminal and outer layers to cell-specific media. The system successfully enabled simultaneous layer-specific cell differentiation in the biomimetic bi-layered vascular graft, effectively replicating the natural architecture and cell phenotypes of native vessels, particularly the tunica intima and tunica media, thanks to its unique design [65].

The major medium absorption by ECM-enriched segments compared with those without, could be explained through the change in macromolecular structure due to the charge shielding effect after immersion. Another possible explanation could be based on the partial molecular release and the loss of crosslinks. Finally, a major porosity in dECM-based bioink could increase DMEM absorption. This result indicates that dECM-based bioprinted vessel can ensure native-like dimensions and good nutrient diffusion within the constructs.

During the degradation test, vascular constructs retained their wall thickness comparable with that of the native aorta upon incubation of 28 days in the medium (Fig. 10 (d)).

This study has established the groundwork for further exploration of functional aspects, such as the interaction with blood, cell-to-cell interactions, and the generation of new tissue guided by biochemical cues derived from the existing matrix.

5. Conclusions

This work presents a novel multi-layered 3D bioprinted construct as an alternative vascular conduit. The design of this dECM-based bioink laid the foundation for a promising alternative for regenerative medicine of tubular constructs with dimensions similar to native tissues. To the best of our knowledge, the bioink characterized by the double-crosslinking of alginate combined with gelatin and decellularized ECM is highly innovative. Moreover, the designed bioink can be employed in 3D bioprinting of self-standing multi-layered aortic-like segments with native dimensions and significant height. The degradation test revealed a slow degradation rate, ensuring prolonged cell support given by the hydrogel. Moreover, the degradation produced porosity, thus potentially promoting vascularization within the construct, when angiogenic drugs are added to the culture medium. Preliminary biological

characterization, carried out by embedding a fibroblast cell line in the dECM bioink, proved cell viability up to 7 days. These results, combined with the mechanical characterization and the easy handling of the printed constructs, encourage the future development of this project, which includes the bioprinting of multi-cellular constructs and their dynamic maturation in a bioreactor under physiological conditions. Moreover, long-term dynamic culture should promote the remodeling of the ECM present in the bioink to mimic the native environment increasingly. In addition, uniaxial tensile tests will be performed on cellularized constructs to evaluate the mechanical properties.

CRediT authorship contribution statement

Federica Potere: Conceptualization, Methodology, Formal analysis, Investigation, Writing - original draft, Visualization. **Giovanni Venturelli:** Conceptualization, Methodology, Formal analysis, Investigation, Writing - original draft, Visualization. **Beatrice Belgio:** Writing, review & editing. **Giuseppe Guagliano:** Investigation and Formal analysis. **Federica Boschetti:** Resources, Writing-review & editing. **Sara Mantero:** Conceptualization, Resources, Writing - review & editing, Supervision, Project Administration. **Paola Petrini:** Conceptualization, Methodology, Resources, Writing - review & editing, Supervision.

Declaration of competing interest

The authors declare that they have no known competing financial interests or personal relationships that could have appeared to influence the work reported in this paper.

Acknowledgments

This research did not receive any specific grant from funding agencies in the public, commercial, or not-for-profit sectors.

Glossary

ECM	extracellular matrix
dECM	decellularized extracellular matrix
Alg-gel bioink	alginate and gelatin bioink
GDL	glucono-δ-lactone
$CaCO_3$	calcium carbonate
$CaCl_2$	alcium chloride dihydrate
DMEM	high glucose Dulbecco's modified eagle's medium
G'	storage modulus
G''	loss modulus
PBS	phosphate-buffered saline
PET	polyethylene-terephthalate
PTFE	polytetrafluoroethylene
ePTFE	expanded polytetrafluoroethylene

Appendix A. Supplementary data

Supplementary data to this article can be found online at https://doi.org/10.1016/j.bprint.2024.e00368.

Data availability

Data will be made available on request.

References

[1] T.K. Brown, S. Alharbi, K.J. Ho, B. Jiang, Prosthetic vascular grafts engineered to combat calcification: progress and future directions, Biotechnol. Bioeng. (2022), https://doi.org/10.1002/bit.28316.
[2] H.A. Mcallister, An Overview of Human Arterial Pathology, Toxicol. Pathol. 17 (1989) 219–231.
[3] L. Li, S. Qin, J. Peng, A. Chen, Y. Nie, T. Liu, K. Song, Engineering gelatin-based alginate/carbon nanotubes blend bioink for direct 3D printing of vessel constructs, Int. J. Biol. Macromol. 145 (2020) 262–271, https://doi.org/10.1016/j.ijbiomac.2019.12.174.
[4] A. Schanzer, G.S. Oderich, Management of abdominal aortic aneurysms, N. Engl. J. Med. 385 (2021) 1690–1698, https://doi.org/10.1056/NEJMcp2108504.
[5] S. Freeman, R. Ramos, P. Alexis Chando, L. Zhou, K. Reeser, S. Jin, P. Soman, K. Ye, A bioink blend for rotary 3D bioprinting tissue engineered small-diameter vascular constructs, Acta Biomater. 95 (2019) 152–164, https://doi.org/10.1016/j.actbio.2019.06.052.
[6] S. Ravi, E.L. Chaikof, Biomaterials for vascular tissue engineering, Regen. Med. 5 (2010) 107–120, https://doi.org/10.2217/rme.09.77.
[7] F. Nappi, A.R. Carotenuto, A. Cutolo, P. Fouret, C. Acar, J.C. Chachques, M. Fraldi, Compliance mismatch and compressive wall stresses drive anomalous remodelling of pulmonary trunks reinforced with Dacron grafts, J. Mech. Behav. Biomed. Mater. 63 (2016) 287–302, https://doi.org/10.1016/j.jmbbm.2016.06.023.
[8] J.S. Soares, S.K. Saunders, F. Potere, S. Toldo, A. Abbate, Engineered tissue vascular grafts: are we there yet? Appl. Eng. Sci. 12 (2022) https://doi.org/10.1016/j.apples.2022.100114.
[9] J.S. Coselli, S.A. Lemaire, Management of Thoracic Aortic Graft Infections, Ann. Thorac. Surg. 67 (1999) 1990–1993.
[10] C.B. Weinberg, E. Bell, A blood vessel model constructed from collagen and cultured vascular cells, Science 231 (1986) 397–400.
[11] Y.M. Ju, J.S. Choi, A. Atala, J.J. Yoo, S.J. Lee, Bilayered scaffold for engineering cellularized blood vessels, Biomaterials 31 (2010) 4313–4321, https://doi.org/10.1016/j.biomaterials.2010.02.002.
[12] J. Jang, H.J. Park, S.W. Kim, H. Kim, J.Y. Park, S.J. Na, H.J. Kim, M.N. Park, S. H. Choi, S.H. Park, S.W. Kim, S.M. Kwon, P.J. Kim, D.W. Cho, 3D printed complex tissue construct using stem cell-laden decellularized extracellular matrix bioinks for cardiac repair, Biomaterials 112 (2017) 264–274, https://doi.org/10.1016/j.biomaterials.2016.10.026.
[13] S. Rayatpisheh, D.E. Heath, A. Shakouri, P.O. Rujitanaroj, S.Y. Chew, M.B. Chan-Park, Combining cell sheet technology and electrospun scaffolding for engineered tubular, aligned, and contractile blood vessels, Biomaterials 35 (2014) 2713–2719, https://doi.org/10.1016/j.biomaterials.2013.12.035.
[14] Z.H. Syedain, L.A. Meier, J.W. Bjork, A. Lee, R.T. Tranquillo, Implantable arterial grafts from human fibroblasts and fibrin using a multi-graft pulsed flow-stretch bioreactor with noninvasive strength monitoring, Biomaterials 32 (2011) 714–722, https://doi.org/10.1016/j.biomaterials.2010.09.019.
[15] A.F. Pellegata, T. Dominioni, F. Ballo, S. Maestroni, M.A. Asnaghi, G. Zerbini, S. Zonta, S. Mantero, Arterial decellularized scaffolds produced using an innovative automatic system, Cells Tissues Organs 200 (2015) 363–373, https://doi.org/10.1159/000439082.
[16] L. Xu, M. Varkey, A. Jorgensen, J. Ju, Q. Jin, J.H. Park, Y. Fu, G. Zhang, D. Ke, W. Zhao, R. Hou, A. Atala, Bioprinting small diameter blood vessel constructs with an endothelial and smooth muscle cell bilayer in a single step, Biofabrication 12 (2020), https://doi.org/10.1088/1758-5090/aba2b6.
[17] T. Gao, G.J. Gillispie, J.S. Copus, A.P.R. Kumar, Y.J. Seol, A. Atala, J.J. Yoo, S. J. Lee, Optimization of gelatin-alginate composite bioink printability using rheological parameters: a systematic approach, Biofabrication 10 (2018), https://doi.org/10.1088/1758-5090/aacdc7.

[18] A. Schwab, R. Levato, M. D'Este, S. Piluso, D. Eglin, J. Malda, Printability and shape fidelity of bioinks in 3D bioprinting, Chem. Rev. 120 (2020) 11028–11055, https://doi.org/10.1021/acs.chemrev.0c00084.

[19] A.S. Moghaddam, H.A. Khonakdar, M. Arjmand, S.H. Jafari, Z. Bagher, Z. S. Moghaddam, M. Chimerad, M.M. Sisakht, S. Shojaei, Review of bioprinting in regenerative medicine: naturally derived bioinks and stem cells, ACS Appl. Bio Mater. 4 (2021) 4049–4070, https://doi.org/10.1021/acsabm.1c00219.

[20] B. Yuan, Y. Jin, Y. Sun, D. Wang, J. Sun, Z. Wang, W. Zhang, X. Jiang, A strategy for depositing different types of cells in three dimensions to mimic tubular structures in tissues, Adv. Mater. 24 (2012) 890–896, https://doi.org/10.1002/adma.201104589.

[21] S. Wüst, M.E. Godla, R. Müller, S. Hofmann, Tunable hydrogel composite with two-step processing in combination with innovative hardware upgrade for cell-based three-dimensional bioprinting, Acta Biomater. 10 (2014) 630–640, https://doi.org/10.1016/j.actbio.2013.10.016.

[22] P.D. Dalton, Melt electrowriting with additive manufacturing principles, Curr. Opin. Biomed. Eng. 2 (2017) 49–57, https://doi.org/10.1016/j.cobme.2017.05.007.

[23] P.S. Gungor-Ozkerim, I. Inci, Y.S. Zhang, A. Khademhosseini, M.R. Dokmeci, Bioinks for 3D bioprinting: an overview, Biomater. Sci. 6 (2018) 915–946, https://doi.org/10.1039/c7bm00765e.

[24] M. Rabionet, A.J. Guerra, T. Puig, J. Ciurana, 3D-printed tubular scaffolds for vascular tissue engineering, in: Procedia CIRP, Elsevier B.V., 2018, pp. 352–357, https://doi.org/10.1016/j.procir.2017.12.094.

[25] J. Xue, T. Wu, Y. Dai, Y. Xia, Electrospinning and electrospun nanofibers: methods, materials, and applications, Chem. Rev. 119 (2019) 5298–5415, https://doi.org/10.1021/acs.chemrev.8b00593.

[26] C.D. Devillard, C.A. Marquette, Vascular tissue engineering: challenges and requirements for an ideal large Scale blood vessel, Front. Bioeng. Biotechnol. 9 (2021), https://doi.org/10.3389/fbioe.2021.721843.

[27] S. Xin, D. Chimene, J.E. Garza, A.K. Gaharwar, D.L. Alge, Clickable PEG hydrogel microspheres as building blocks for 3D bioprinting, Biomater. Sci. 7 (2019) 1179–1187, https://doi.org/10.1039/c8bm01286e.

[28] M. Nowicki, W. Zhu, K. Sarkar, R. Rao, L.G. Zhang, 3D printing multiphasic osteochondral tissue constructs with nano to micro features via PCL based bioink, Bioprinting 17 (2020), https://doi.org/10.1016/j.bprint.2019.e00066.

[29] M.S. Izgordu, E.I. Uzgur, S. Ulag, A. Sahin, B. Karademir Yilmaz, B. Kilic, N. Ekren, F.N. Oktar, O. Gunduz, Investigation of 3D-printed polycaprolactone-/polyvinylpyrrolidone-based constructs, Cartilage 13 (2021) 626S–635S, https://doi.org/10.1177/1947603519897302.

[30] R. Khoeini, H. Nosrati, A. Akbarzadeh, A. Eftekhari, T. Kavetskyy, R. Khalilov, E. Ahmadian, A. Nasibova, P. Datta, L. Roshangar, D.C. Deluca, S. Davaran, M. Cucchiarini, I.T. Ozbolat, Natural and synthetic bioinks for 3D bioprinting, Adv. Nanobiomed. Res. 1 (2021), https://doi.org/10.1002/anbr.202000097.

[31] D.F. Duarte Campos, A. Blaeser, M. Weber, J. Jäkel, S. Neuss, W. Jahnen-Dechent, H. Fischer, Three-dimensional printing of stem cell-laden hydrogels submerged in a hydrophobic high-density fluid, Biofabrication 5 (2013), https://doi.org/10.1088/1758-5082/5/1/015003.

[32] F. Iervolino, B. Belgio, A. Bonessa, F. Potere, R. Suriano, F. Boschetti, S. Mantero, M. Levi, Versatile and non-cytotoxic GelMA-xanthan gum biomaterial ink for extrusion-based 3D bioprinting, Bioprinting 31 (2023), https://doi.org/10.1016/j.bprint.2023.e00269.

[33] Y.S.E. Tan, W.Y. Yeong, Direct bioprinting of alginate-based tubular constructs using multi-nozzle extrusion-based technique, in: Proceedings of the International Conference on Progress in Additive Manufacturing, Pro-AM, 2014, pp. 423–427, https://doi.org/10.3850/978-981-09-0446-3_093.

[34] A.G. Tabriz, M.A. Hermida, N.R. Leslie, W. Shu, Three-dimensional bioprinting of complex cell laden alginate hydrogel structures, Biofabrication 7 (2015), https://doi.org/10.1088/1758-5090/7/4/045012.

[35] H. Ding, R.C. Chang, Printability study of bioprinted tubular structures using liquid hydrogel precursors in a support bath, Appl. Sci. 8 (2018), https://doi.org/10.3390/app8030403.

[36] K.A. Gold, B. Saha, N.K. Rajeeva Pandian, B.K. Walther, J.A. Palma, J. Jo, J. P. Cooke, A. Jain, A.K. Gaharwar, 3D bioprinted multicellular vascular models, Adv. Healthcare Mater. 10 (2021), https://doi.org/10.1002/adhm.202101141.

[37] C. Dikyol, M. Altunbek, B. Koc, Embedded multimaterial bioprinting platform for biofabrication of biomimetic vascular structures, J. Mater. Res. 36 (2021) 3851–3864, https://doi.org/10.1557/s43578-021-00254-x.

[38] H. Liu, X. Yang, X. Cheng, G. Zhao, G. Zheng, X. Li, R. Dong, Theoretical and experimental research on multi-layer vessel-like structure printing based on 3D bio-printing technology, Micromachines 12 (2021), https://doi.org/10.3390/mi12121517.

[39] A.F. Pellegata, M. Adelaide Asnaghi, S. Zonta, G. Zerbini, S. Mantero, A novel device for the automatic decellularization of biological tissues, Int. J. Artif. Organs 35 (2012) 191–198, https://doi.org/10.5301/ijao.5000079.

[40] J. Jang, T.G. Kim, B.S. Kim, S.W. Kim, S.M. Kwon, D.W. Cho, Tailoring mechanical properties of decellularized extracellular matrix bioink by vitamin B2-induced photo-crosslinking, Acta Biomater. 33 (2016) 88–95, https://doi.org/10.1016/j.actbio.2016.01.013.

[41] M. Carrabba, P. Madeddu, Current strategies for the manufacture of small size tissue engineering vascular grafts, Front. Bioeng. Biotechnol. 6 (2018), https://doi.org/10.3389/fbioe.2018.00041.

[42] F. Potere, B. Belgio, G.A. Croci, S. Tabano, P. Petrini, G. Dubini, F. Boschetti, S. Mantero, 3D bioprinting of multi-layered segments of a vessel-like structure with ECM and novel derived bioink, Front. Bioeng. Biotechnol. 10 (2022), https://doi.org/10.3389/fbioe.2022.918690.

[43] D.O. Freytes, J. Martin, S.S. Velankar, A.S. Lee, S.F. Badylak, Preparation and rheological characterization of a gel form of the porcine urinary bladder matrix, Biomaterials 29 (2008) 1630–1637, https://doi.org/10.1016/j.biomaterials.2007.12.014.

[44] F. Pati, D.H. Ha, J. Jang, H.H. Han, J.W. Rhie, D.W. Cho, Biomimetic 3D tissue printing for soft tissue regeneration, Biomaterials 62 (2015) 164–175, https://doi.org/10.1016/j.biomaterials.2015.05.043.

[45] L. Sardelli, M. Tunesi, F. Briatico-Vangosa, P. Petrini, 3D-Reactive printing of engineered alginate inks, Soft Matter 17 (2021) 8105–8117, https://doi.org/10.1039/d1sm00604e.

[46] J. Hazur, R. Detsch, E. Karakaya, J. Kaschta, J. Teßmar, D. Schneidereit, O. Friedrich, D.W. Schubert, A.R. Boccaccini, Improving alginate printability for biofabrication: establishment of a universal and homogeneous pre-crosslinking technique, Biofabrication 12 (2020), https://doi.org/10.1088/1758-5090/ab98e5.

[47] L. Ouyang, R. Yao, Y. Zhao, W. Sun, Effect of bioink properties on printability and cell viability for 3D bioplotting of embryonic stem cells, Biofabrication 8 (2016), https://doi.org/10.1088/1758-5090/8/3/035020.

[48] D. Therriault, S.R. White, J.A. Lewis, Rheological behavior of fugitive organic inks for direct-write assembly, Appl. Rheol. 17 (2007) 10112-1–10112-8.

[49] A. Ribeiro, M.M. Blokzijl, R. Levato, C.W. Visser, M. Castilho, W.E. Hennink, T. Vermonden, J. Malda, Assessing bioink shape fidelity to aid material development in 3D bioprinting, Biofabrication 10 (2018), https://doi.org/10.1088/1758-5090/aa90e2.

[50] F. Kabirian, M. Mozafari, Decellularized ECM-derived bioinks: prospects for the future, Methods 171 (2020) 108–118, https://doi.org/10.1016/j.ymeth.2019.04.019.

[51] L. Edgar, T. Pu, B. Porter, J.M. Aziz, C. La Pointe, A. Asthana, G. Orlando, Regenerative medicine, organ bioengineering and transplantation, Br. J. Surg. 107 (2020) 793–800, https://doi.org/10.1002/bjs.11686.

[52] G. Guagliano, C. Volpini, F. Briatico-Vangosa, A.I. Cornaglia, L. Visai, P. Petrini, Toward 3D-bioprinted models of the liver to boost drug development, Macromol. Biosci. 22 (2022), https://doi.org/10.1002/mabi.202200264.

[53] X. Ma, C. Yu, P. Wang, W. Xu, X. Wan, C.S.E. Lai, J. Liu, A. Koroleva-Maharajh, S. Chen, Rapid 3D bioprinting of decellularized extracellular matrix with regionally varied mechanical properties and biomimetic microarchitecture, Biomaterials 185 (2018) 310–321, https://doi.org/10.1016/j.biomaterials.2018.09.026.

[54] G. Guagliano, C. Volpini, L. Sardelli, N. Bloise, F. Briatico-Vangosa, A.I. Cornaglia, S. Dotti, R. Villa, L. Visai, P. Petrini, Hep3Gel: a shape-shifting extracellular matrix-based, three-dimensional liver model adaptable to different culture systems, ACS Biomater. Sci. Eng. 9 (2023) 211–229, https://doi.org/10.1021/acsbiomaterials.2c01226.

[55] X. Zhang, Y. Liu, C. Luo, C. Zhai, Z. Li, Y. Zhang, T. Yuan, S. Dong, J. Zhang, W. Fan, Crosslinker-free silk/decellularized extracellular matrix porous bioink for 3D bioprinting-based cartilage tissue engineering, Mater. Sci. Eng. C 118 (2021), https://doi.org/10.1016/j.msec.2020.111388.

[56] C. Yu, X. Ma, W. Zhu, P. Wang, K.L. Miller, J. Stupin, A. Koroleva-Maharajh, A. Hairabedian, S. Chen, Scanningless and continuous 3D bioprinting of human tissues with decellularized extracellular matrix, Biomaterials 194 (2019) 1–13, https://doi.org/10.1016/j.biomaterials.2018.12.009.

[57] I. Yuki, I. Kan, A. Golshan, J. Sohn, Y. Murayama, H.V. Vinters, F. Viñuela, A swine model to analyze arterial structural changes induced by mechanical thrombectomy, Am. J. Neuroradiol. 34 (2013), https://doi.org/10.3174/ajnr.A3221.

[58] A. Goins, A.R. Webb, J.B. Allen, Multi-layer approaches to scaffold-based small diameter vessel engineering: a review, Mater. Sci. Eng. C 97 (2019) 896–912, https://doi.org/10.1016/j.msec.2018.12.067.

[59] M. Müller, J. Becher, M. Schnabelrauch, M. Zenobi-Wong, Nanostructured Pluronic hydrogels as bioinks for 3D bioprinting, Biofabrication 7 (2015), https://doi.org/10.1088/1758-5090/7/3/035006.

[60] A.A. Zadpoor, Bone tissue regeneration: the role of scaffold geometry, Biomater. Sci. 3 (2015) 231–245, https://doi.org/10.1039/c4bm00291a.

[61] P. Han, G.A. Gomez, G.N. Duda, S. Ivanovski, P.S.P. Poh, Scaffold geometry modulation of mechanotransduction and its influence on epigenetics, Acta Biomater. (2022), https://doi.org/10.1016/j.actbio.2022.01.020.

[62] S. Mantero, N. Sadr, S.A. Riboldi, S. Lorenzoni, F.M. Montevecchi, A new electro-mechanical bioreactor for soft tissue engineering, J Appl Biomater Biomech 5 (2007) 107–116.

[63] D. Lim, E.S. Renteria, D.S. Sime, Y.M. Ju, J.H. Kim, T. Criswell, T.D. Shupe, A. Atala, F.C. Marini, M.N. Gurcan, S. Soker, J. Hunsberger, J.J. Yoo, Bioreactor design and validation for manufacturing strategies in tissue engineering, Biodes Manuf 5 (2022) 43–63, https://doi.org/10.1007/s42242-021-00154-3.

[64] C.D. Devillard, C.A. Marquette, Vascular tissue engineering: challenges and requirements for an ideal large Scale blood vessel, Front. Bioeng. Biotechnol. 9 (2021), https://doi.org/10.3389/fbioe.2021.721843.

[65] I. Pennings, E.E. Van Haaften, T. Jungst, J.A. Bulsink, A.J.W.P. Rosenberg, J. Groll, C.V.C. Bouten, N.A. Kurniawan, A.I.P.M. Smits, D. Gawlitta, Layer-specific cell differentiation in bi-layered vascular grafts under flow perfusion, Biofabrication 12 (2020), https://doi.org/10.1088/1758-5090/ab47f0.

[66] N. Bono, S. Meghezi, M. Soncini, M. Piola, D. Mantovani, G.B. Fiore, A dual-mode bioreactor system for tissue engineered vascular models, Ann. Biomed. Eng. 45 (2017) 1496–1510, https://doi.org/10.1007/s10439-017-1813-9.